

Exact solution for square-wave grating covered with graphene: Surface plasmon-polaritons in the THz range

N. M. R. Peres¹, Yu. V. Bludov¹, Aires Ferreira², and M. I. Vasilevskiy¹

¹*Department of Physics and Center of Physics, University of Minho, Campus de Gualtar, P-4710-057, Braga, Portugal and*

²*Graphene Research Centre and Department of Physics, National University of Singapore, 2 Science Drive 3, Singapore 117542*

(Dated: September 5, 2021)

We provide an analytical solution to the problem of scattering of electromagnetic radiation by a square-wave grating with a flat graphene sheet on top. We show that for deep grooves there is a strong plasmonic response with light absorption in the graphene sheet reaching more than 45%, due to the excitation of surface plasmon-polaritons. The case of grating with a graphene sheet presenting an induced periodic modulation of the conductivity is also discussed.

PACS numbers: 81.05.ue,78.67.-n,78.30.-j

I. INTRODUCTION

Plasmonic effects in graphene is currently an active research topic. The strong plasmonic response of graphene at room temperature is tied up to its optical response, which can be controlled externally in different ways. The unique features of the optical conductivity of single-layer graphene stem from the Dirac-like nature of quasi-particles,¹⁻³ and have been extensively studied in the past few years, both theoretically^{1,2,4-16} and experimentally,¹⁷⁻²⁴ including in the terahertz (THz) spectral range.²⁵⁻²⁸

Indeed graphene holds many promises for cutting edge THz applications,²⁹ which would be able to fill the so called *THz gap*. More recently the interest has been focused to how graphene interacts with electromagnetic radiation in the THz.³⁰⁻³⁶ One of the goals is to enhance the absorption of graphene for the development of more efficient photodetectors in that spectral range. This can be done in several different ways, by (i) producing micro-disks of graphene on a layered structure,³⁰ (ii) exploiting the physics of quantum dots and metallic arrays on graphene;^{32,37} (iii) using a graphene based grating;³⁸⁻⁴¹ (iv) putting graphene inside an optical cavity;^{42,43} and (v) depositing graphene on a photonic crystal.¹⁵ In cases (i), (ii), and (iii) the excitation of plasmons⁴⁴⁻⁴⁷ is responsible for the enhancement of the absorption. In case (iv) photons undergo many round trips inside the cavity enhancing the chances of being absorbed by graphene. In case (v) the authors consider a photonic crystal made of SiO₂/Si. In the visible range of the spectrum the dielectric constants of SiO₂ and Si differ by more than one order of magnitude and choosing the width of the SiO₂/Si appropriately it is possible to induce a large photonic band gap in the visible range. Combining the presence of the band gap with an initial spacer layer the absorption can be enhanced by a factor of four. In the case studied in Ref. 15 the optical conductivity of graphene is controlled by interband transitions. Although this work¹⁵ focused on the visible spectrum, there is *a priori* no reason why the same principle cannot be extended to the THz.

The physics of surface plasmon-polaritons in graphene has also been explored for the development of devices for optoelectronic applications.⁴⁸⁻⁵⁰ Such devices include optical switches⁵¹ and polarizers.⁵² It has been shown that metallic single-wall carbon nanotubes, which have a linear spectrum close to zero energy, can act as polarizers as well.²⁷ Theoretical studies of the optical response of graphene under intense THz radiation has also been performed.⁵³⁻⁵⁶

In general, the conductivity of graphene is a sum of two contributions: (i) a Drude-type term, describing intraband processes and (ii) a term describing interband transitions. At zero temperature the optical conductivity has a simple analytical expression.^{1,2,4,5,8,57} In what concerns our study, the physics of the system is dominated by the intraband contribution,⁵⁸ which reads

$$\sigma_D = \sigma_0 \frac{4E_F}{\pi} \frac{1}{\hbar\Gamma - i\hbar\omega}, \quad (1)$$

where, $\sigma_0 = \pi e^2 / (2h)$, Γ is the relaxation rate, $E_F > 0$ is the Fermi level position with respect to the Dirac point, and ω is the radiation frequency. It should be noted that σ_D has a strong frequency dependence and is responsible for the optical behaviour of graphene in the THz spectral range.

The problem we consider in this work is the scattering of electromagnetic radiation by graphene deposited on a grating with a square-wave profile, as illustrated in Fig. 1. We further assume that the radiation is *p*-polarized (TM wave), that is, we take $\mathbf{B} = (0, B_y, 0)$ and $\mathbf{E} = (E_x, 0, E_z)$. The square-wave profile is rather pathologic due to the infinite derivative at the edges of the steps and therefore the usual methods fail.^{38,40,59,60} An alternative route is to obtain the exact eigenfunctions in the region of the grooves.⁶¹ Fortunately, the geometry of the problem is equivalent to that of a Kronig-Penney model appearing in the band theory of solids and for which an exact solution exists. We will show that Maxwell's equations can be put in a form equivalent to the Schrödinger equation for the Kronig-Penney model, and hence an exact solution for the fields in the region of

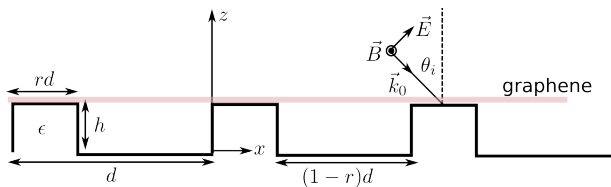


FIG. 1: Geometry of the problem. The incident angle is θ_i and the incoming wave number is \mathbf{k}_0 . The radiation is p -polarized. A top gate for the electrostatic doping of graphene can be arranged as a transparent electrode placed at some distance above the graphene sheet. Alternatively, a bottom gate can be placed below the dielectric substrate.

the grooves is possible.

In this work we assume that graphene is doped. In a practical implementation, this can be achieved via gating or by chemical means.^{62,63} Remark that in a bottom gate structure the conductivity of graphene becomes position dependent along the x -direction.³⁸ In this case, the analysis presented below is incomplete (see, however, Sec. VI, where a simplified model is analysed). Nevertheless, the results of Ref. 38 show that a position dependent conductivity alone already induces surface plasmon-polaritons on graphene. Therefore, a spatially modulated optical response, when combined with a grating, will enhance the excitation of surface plasmon-polaritons, as confirmed by the analysis given in Sec. VI. For the top gate configuration and for chemical doping, the problem of a spatial dependent conductivity does not arise.⁶⁴

It can be argued that in the geometry we are considering (see Fig. 1) the portion of graphene over the grooves will be strained. Clearly, experimental setups can be designed as to overcome (at least partially) such effects e.g., by filling the grooves with a different dielectric and using a top gate or a chemically doped graphene. However, in the bottom gate configuration, even with filled grooves, graphene will have a position dependent conductivity. A complete description should thus include all contributions: the grating effect itself, inhomogeneous doping, and the strain fields in graphene. In this work we assume that the graphene sheet remains flat. First, the optical conductivity will be taken homogeneous in order to study solely the effect of dielectric grating in the presence of uniform graphene. The additional effect of periodic modulation of the graphene conductivity, with the same period as the grating, will be considered in Sec. VI. We believe that our calculations are accurate for the cases of either electrostatic doping by a top gate,⁶⁴ or doping by chemical means.^{62,63}

II. EXACT EIGENMODES IN THE GRATING REGION

For TM polarized light with angular frequency ω (see Fig. 1) the Helmholtz equation assumes the simple form

$$(\Delta_{\parallel} + \mu_0 \epsilon \omega^2) B_y(x, z) = 0, \quad (2)$$

where μ_0 is the vacuum permeability and $\Delta_{\parallel} = \partial_x^2 + \partial_z^2$. Since the boundary between the vacuum and the dielectric is piecewise, the Helmholtz equation holds true in the regions of width rd and $(1-r)d$ with the appropriate change of the dielectric constant, ϵ in the former and ϵ_0 in the latter. For $z > h$ the dielectric constant is homogeneous and equal to ϵ_0 , whereas for $z < 0$ it is $\epsilon = \epsilon_0 \epsilon_r$, and ϵ_r is the relative permittivity.

We search solutions of Eq. 2 in the form

$$B_y = B_y(x, z) = X(x) e^{\pm i \Lambda z}, \quad (3)$$

where Λ is a constant. With this ansatz, the Helmholtz equation reduces to

$$\partial_x^2 X(x) = (\Lambda - \mu_0 \epsilon \omega^2) X(x), \quad (4)$$

whose solution is

$$X(x) = A_j e^{ik_j x} + B_j e^{-ik_j x}, \quad (5)$$

and where k_j^2 is given by

$$k_j^2 = \mu_0 \epsilon_j \omega^2 - \Lambda^2, \quad (6)$$

with the subscript $j = 1$ [$j = 2$] referring to the region $(1-r)d$ [rd]. Putting all pieces together, the field component B_y in the regions of the grooves reads

$$B_y^{(j)} = [A_j e^{ik_j x} + B_j e^{-ik_j x}] e^{\pm i \Lambda z}. \quad (7)$$

The determination of Λ in Eq. (7) leads to an eigenvalue problem that will be considered in the next section. We note that Λ can be either real or pure imaginary: real values correspond to propagating diffracted orders, whereas imaginary ones correspond to evanescent waves. From Maxwell's equations it follows that the electric field components in the region $0 < z < d$ read:

$$E_x^{(j)} = \frac{\pm \Lambda}{\mu_0 \epsilon_j \omega} [A_j e^{ik_j x} + B_j e^{-ik_j x}] e^{\pm i \Lambda z}, \quad (8)$$

$$E_z^{(j)} = \frac{-k_j}{\mu_0 \epsilon_j \omega} [A_j e^{ik_j x} - B_j e^{-ik_j x}] e^{\pm i \Lambda z}. \quad (9)$$

As shown in what follows, there is a relation between the coefficients A_j and B_j , which is obtained from the solution of the eigenvalue problem.

III. TRANSFER MATRIX AND THE EIGENVALUE EQUATION

Along the x -direction, and for $0 < z < h$, we have a stratified medium with alternating dielectric constants.

Then we can relate the amplitudes A_j and B_j with A_{j+1} and B_{j+1} using the boundary conditions at the interfaces of the two dielectrics. Furthermore, using the Bloch theorem we can find an eigenvalue equation for the parameter Λ . The amplitudes in the different regions of the stratified medium are represented in Fig. 2. The continuity

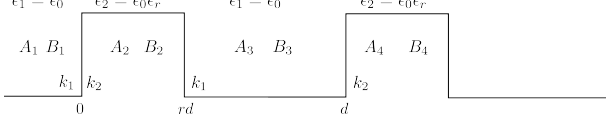


FIG. 2: Effective stratified medium along the x -direction in the region $0 < z < h$.

of the z -component of the electric field at the boundary $x = rd$ imposes a relation between the amplitudes A and B in regions $j = 2, 3$ (refer to Fig. 2 for the definition of the different regions), i.e.,

$$\frac{k_2}{\epsilon_r} [A_2 e^{ik_2 rd} - B_2 e^{-ik_2 rd}] = k_1 [A_3 e^{ik_1 rd} - B_3 e^{-ik_1 rd}]. \quad (10)$$

Note that according to the definition in Eq. (6), we must have $k_3 = k_1$ and $k_4 = k_2$. At the same boundary, the continuity of the magnetic field yields

$$A_2 e^{ik_2 rd} + B_2 e^{-ik_2 rd} = A_3 e^{ik_1 rd} + B_3 e^{-ik_1 rd}. \quad (11)$$

It is convenient to write these two equations in matrix form as follows

$$\begin{bmatrix} A_2 \\ B_2 \end{bmatrix} = \Phi(k_2 rd) K_2^{-1} K_1 \Phi(-k_1 rd) \begin{bmatrix} A_3 \\ B_3 \end{bmatrix}, \quad (12)$$

where

$$\Phi(x) = \begin{bmatrix} e^{-ix} & 0 \\ 0 & e^{ix} \end{bmatrix}, \quad (13)$$

$$K_1 = \begin{bmatrix} k_1 & -k_1 \\ 1 & 1 \end{bmatrix}, \quad (14)$$

$$K_2 = \begin{bmatrix} k_2/\epsilon_r & -k_2/\epsilon_r \\ 1 & 1 \end{bmatrix}. \quad (15)$$

Similar continuity conditions apply to the boundary at $x = d$, resulting in the following constraints

$$k_1 [A_3 e^{ik_1 d} - B_3 e^{-ik_1 d}] = \frac{k_2}{\epsilon_r} [A_4 e^{ik_2 d} - B_4 e^{-ik_2 d}], \quad (16)$$

$$A_3 e^{ik_1 d} + B_3 e^{-ik_1 d} = A_4 e^{ik_2 d} + B_4 e^{-ik_2 d}. \quad (17)$$

As before, these equations can be written in matrix form as

$$\begin{bmatrix} A_3 \\ B_3 \end{bmatrix} = \Phi(k_1 d) K_1^{-1} K_2 \Phi(-k_2 d) \begin{bmatrix} A_4 \\ B_4 \end{bmatrix}, \quad (18)$$

Combining Eqs. (12) and (18), we arrive at the following result

$$\begin{bmatrix} A_2 \\ B_2 \end{bmatrix} = \Phi(k_2 rd) K_2^{-1} K_1 \Phi[k_1 d(1-r)] K_1^{-1} K_2 \times \begin{bmatrix} A_4 \\ B_4 \end{bmatrix}, \quad (19)$$

where a global phase was absorbed in the coefficients A_4 and B_4 . The transfer matrix,

$$T = [\Phi(k_2 rd) K_2^{-1} K_1 \Phi[k_1 d(1-r)] K_1^{-1} K_2]^{-1}, \quad (20)$$

propagates the field amplitudes through the 1D crystal in the x -direction,

$$\begin{bmatrix} A_4 \\ B_4 \end{bmatrix} = T \begin{bmatrix} A_2 \\ B_2 \end{bmatrix}. \quad (21)$$

[Note that $\det(T) = 1$.] On the other hand, by virtue of the Bloch theorem we have:

$$\begin{bmatrix} A_4 \\ B_4 \end{bmatrix} = e^{ik_0 d \sin \theta_i} \begin{bmatrix} A_2 \\ B_2 \end{bmatrix}, \quad (22)$$

where $k_0 \sin \theta_i$ is the x -component of the wavevector of the incoming electromagnetic radiation (Fig. 1). We thus arrive at the important intermediate result

$$e^{ik_0 d \sin \theta_i} \begin{bmatrix} A_2 \\ B_2 \end{bmatrix} = T \begin{bmatrix} A_2 \\ B_2 \end{bmatrix}. \quad (23)$$

The compatibility condition of Eq. (23) provides the eigenvalue equation

$$2 \cos(k_0 d \sin \theta_i) = \text{Tr}(T), \quad (24)$$

or explicitly,

$$2 \cos(k_0 d \sin \theta_i) = 2 \cos[k_1 d(1-r)] \cos(k_2 dr) - \frac{\epsilon_r^2 k_1^2 + k_2^2}{\epsilon_r k_1 k_2} \sin[k_1 d(1-r)] \sin(k_2 dr). \quad (25)$$

Eq. (25) allows for the determination of the permitted values of Λ^2 and is very similar to the eigenvalue equation of the Kronig-Penney model of electron bands.

The relation (12) allows us to express the coefficients A_3 and B_3 in terms of A_2 and B_2 . Thus, the function $X(x)$ over the whole unit cell can be written in terms of A_2 and B_2 only. Furthermore, Eq. (23) gives a relation between the coefficient A_2 and B_2 ,

$$B_2 = \frac{-T_{11} + e^{ik_0 d \sin \theta_i}}{T_{12}} A_2, \quad (26)$$

where T_{12} and T_{22} are two matrix elements of the transfer matrix T . Therefore, the function $X(x)$ over the unit cell is proportional to the only coefficient, A_2 . Note that the matrix elements contain Λ^2 , therefore we shall label the possible functions $X(x)$ by index ℓ running over all

possible eigenvalues ($\pm\Lambda_\ell$). The function $X_\ell(x)$ in a unit cell has the form

$$X_\ell(x) = \begin{cases} A_2 e^{ik_2 x} + B_2 e^{-ik_2 x}, & 0 < x < rd, \\ A_3 e^{ik_1 x} + B_3 e^{-ik_1 x}, & rd < x < d. \end{cases} \quad (27)$$

Equation (12) can be writtent explicitly as

$$\begin{aligned} A_3 &= aA_2 + bB_2, \\ B_3 &= cA_2 + fB_2, \end{aligned}$$

where

$$\begin{aligned} a &= \frac{1}{2k_1 \epsilon_r} e^{-i(k_1 - k_2)rd} (k_2 + k_1 \epsilon_r), \\ f &= \frac{1}{2k_1 \epsilon_r} e^{i(k_1 - k_2)rd} (k_2 + k_1 \epsilon_r), \\ b &= \frac{1}{2k_1 \epsilon_r} e^{-i(k_1 + k_2)rd} (-k_2 + k_1 \epsilon_r), \\ c &= \frac{1}{2k_1 \epsilon_r} e^{i(k_1 + k_2)rd} (-k_2 + k_1 \epsilon_r). \end{aligned}$$

Since the wave numbers k_j can be complex, f is not necessarily the complex conjugate of a ; the same applies to b and c . In terms of these coefficients, $X_\ell(x)$ reads:

$$X_\ell(x) = \begin{cases} A_2 e^{ik_2 x} + B_2 e^{-ik_2 x}, & 0 < x < rd, \\ (aA_2 + bB_2) e^{ik_1 x} + \\ (cA_2 + fB_2) e^{-ik_1 x}, & rd < x < d. \end{cases} \quad (28)$$

We also note that Eq. (26) allows to replace B_2 in Eq. (28). Finally, the magnetic field in the region $0 < z < h$ (hereafter denoted as region II) has the form,

$$B_y^{II} = \sum_{\ell} X_\ell(x) (C_\ell e^{i\Lambda_\ell z} + D_\ell e^{-i\Lambda_\ell z}), \quad (29)$$

where the summation is over all the eigenvalues determined from the solution of Eq. (25) and C_ℓ and D_ℓ are some coefficients that will be determined in the next section. With this we conclude the exact solution for the eigenmodes in the grating region.

IV. SOLUTION OF THE SCATTERING PROBLEM

We now derive the equations for the scattering problem represented in Fig. 1. For $z > h$ (region I) the magnetic field is written as

$$B_y^I = e^{i(\alpha_0 x - \beta_0^{(1)} z)} + \sum_{n=-\infty}^{\infty} R_n e^{i(\alpha_n x + \beta_n^{(1)} z)}, \quad (30)$$

and for $z < 0$ (region III) we have

$$B_y^{III} = \sum_{n=-\infty}^{\infty} T_n e^{i(\alpha_n x - \beta_n^{(2)} z)}, \quad (31)$$

where

$$\alpha_n = k_0 \sin \theta_i - 2\pi n/d, \quad (32)$$

$$\beta_n^{(p)} = \begin{cases} \sqrt{q_p^2 - \alpha_n^2}; & q_p \geq \alpha_n \\ i\sqrt{\alpha_n^2 - q_p^2}; & q_p < \alpha_n \end{cases}, \quad (33)$$

with $q_p = \omega/v_p$ and the definition $q_1 = k_0$; n is an integer, $n \in [-\infty, \infty]$. Since we have four sets of unknown amplitudes, C_ℓ , D_ℓ , R_n , and T_n , and four boundary conditions, two at $z = h$ and other two at $z = 0$, we have a linear system of equations that can be solved in closed form if truncated to some finite order, N_ℓ , which is the number of the eigenvalues needed in Eq. (29) for an accurate description of B_y^{II} (we typically used $N_\ell \sim 20$).

The boundary conditions at $z = 0$ are

$$E_x^{III}(x, z=0) = E_x^{II}(x, z=0), \quad (34)$$

$$B_y^{III}(x, z=0) = B_y^{II}(x, z=0), \quad (35)$$

whereas those at $z = h$ read

$$E_x^I(x, z=h) = E_x^{II}(x, z=h), \quad (36)$$

$$\begin{aligned} B_y^I(x, z=h) - B_y^{II}(x, z=h) = \\ - \mu_0 \sigma_D E_x^{II}(x, z=h). \end{aligned} \quad (37)$$

The latter represents the magnetic field discontinuity across the graphene sheet.⁵¹

These boundary conditions are x dependent. Since the system has period d , we can eliminate this dependence by multiplying the boundary conditions by $e^{-i\alpha_m x}$ and integrating over the unit cell. After some algebra, we arrive at

$$\sum_{\ell=1}^{N_\ell} (f_{\ell m}^{(+)} C_\ell + f_{\ell m}^{(-)} D_\ell) = 0, \quad (38)$$

$$\sum_{\ell=1}^{N_\ell} (g_{\ell m}^{(+)} C_\ell + g_{\ell m}^{(-)} D_\ell) = 2e^{-i\beta_0^{(1)} h} \delta_{m,0}, \quad (39)$$

where

$$f_{\ell m}^{(\pm)} = \frac{\beta_m^{(2)}}{\epsilon} \chi_{\ell m} \pm \Omega_{\ell m} \Lambda_\ell,$$

$$g_{\ell m}^{(\pm)} = \left(\chi_{\ell m} \mp \frac{\sigma_D}{\omega} \Omega_{\ell m} \Lambda_\ell \mp \epsilon_0 \Omega_{\ell m} \frac{\Lambda_\ell}{\beta_m^{(1)}} \right) e^{\pm i\Lambda_\ell h},$$

with

$$\chi_{\ell m} = \frac{1}{d} \int_0^d dx X_\ell(x) e^{-i\alpha_m x}, \quad (40)$$

$$\Omega_{\ell m} = \frac{1}{d} \int_0^d dx \frac{X_\ell(x)}{\epsilon(x)} e^{-i\alpha_m x}. \quad (41)$$

Here $\epsilon(x)$ is defined as $\epsilon[\epsilon_0]$ for $x = rd[d(1-r)]$. Eqs. (38) and (39) form a linear system of equations for the amplitudes C_ℓ and D_ℓ , from which the reflectance and transmittance can be computed. Taking N_ℓ odd, the integer m

belongs to the interval $m \in [-(N_\ell-1)/2, (N_\ell-1)/2]$. The transmittance and the reflectance amplitudes are given by

$$T_m = \sum_{\ell=1}^{N_\ell} \chi_{\ell m} (C_\ell + D_\ell), \quad (42)$$

$$R_m = \delta_{0,m} e^{-2i\beta_0^{(1)}h} + e^{-i\beta_m^{(1)}h} \times \sum_{\ell=1}^{N_\ell} \epsilon_0 \Omega_{\ell m} \frac{\Lambda_\ell}{\beta_m^{(1)}} (C_\ell e^{i\Lambda_\ell h} - D_\ell e^{-i\Lambda_\ell h}). \quad (43)$$

Since $X_\ell(x)$ is a sum of exponentials, the functions $\chi_{\ell m}$ and $\Omega_{\ell m}$ can be determined in closed form, which saves computational power. Explicit equations for $\chi_{\ell m}$ and $\Omega_{\ell m}$ are given in the Appendix A.

V. RESULTS FOR HOMOGENEOUS GRAPHENE

We now provide a number of results obtained from the solution of Eqs. (38) and (39). In Fig. 3 we depict the absorbance (a), reflectance (b), and transmittance (c) at normal incidence. For the parameters considered only the specular order exists; all the other diffraction orders are evanescent. Then, the absorbance is defined as

$$\mathcal{A} = 1 - |R_0|^2 - \frac{\beta_0^{(2)}}{\epsilon_r \beta_0^{(1)}} |T_0|^2. \quad (44)$$

A resonance is clearly seen in the absorbance curves at a frequency of about 16 meV, corresponding to the excitation of a surface plasmon-polariton. The position of the resonance depends on several parameters, given in the caption of Fig. 3 and chosen as typical values appropriate for THz physics. The thin dashed curve corresponds to graphene on a homogeneous dielectric (no grating, $r = 1$). The effect of increasing the depth of the grooves, from $h = d/10$ up to $h = d$ is to produce an enhancement of the absorption, which for $h = d$ is almost of 25% (in this case we are considering $r = 0.25$).

The dispersion of a surface plasmon-polaritons in graphene, when the sheet is sandwiched between two semi-infinite dielectrics, is, in the electrostatic limit, given by³⁸

$$\hbar\omega = \sqrt{2\alpha_f^{(\bar{\epsilon})} E_F \hbar c q}, \quad (45)$$

where

$$\alpha_f^{(\bar{\epsilon})} = \frac{e^2}{4\pi\bar{\epsilon}\hbar c}, \quad (46)$$

and $\bar{\epsilon} = \epsilon_0(1 + \epsilon_r)/2$. Taking $q = 2\pi/d$, the smallest lattice wavevector, Eq. (45) predicts, for the parameters used in our calculation, a plasmon-polariton energy of

$$\hbar\omega = 12.1 \text{ meV}, \quad (47)$$

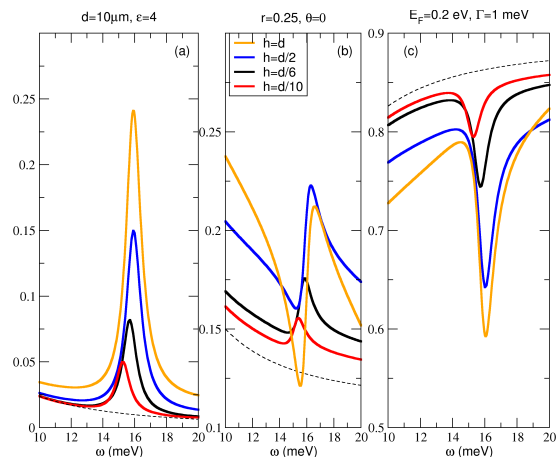


FIG. 3: Absorbance (a), reflectance (b), and transmittance (c) at normal incidence. The parameters are $E_F = 0.2$ eV, $d = 10 \mu\text{m}$, $r = 0.25$, $\theta_i = 0$, $\epsilon_r = 4$ (corresponding to SiO_2), and $\Gamma = 1$ meV. The thin dashed line is the case $r = 1$. For reference, we note that 1 THz corresponds to an energy of 4.1 meV.

which is in the ballpark of the numeric result. We should however note that the position of the resonance depends also on the parameter r , which is not captured by the above formula for the dispersion. We can include the effect of the parameter r using an interpolative formula. We define a new $\bar{\epsilon}$ as

$$\bar{\epsilon} = \frac{\epsilon_0}{2} (2 - r + \epsilon_r r). \quad (48)$$

Using this formula we obtain

$$\hbar\omega = 16.3 \text{ meV}, \quad (49)$$

a much better approximation to the numerical value (15.9 meV). To obtain the exact frequency of the resonance we have to compute the plasmonic band structure due to the periodic dielectric, that is, the band structure of a polaritonic crystal.³⁹ In the Appendix B we give the polaritonic band structure of graphene on a square-wave grating.

In Fig. 4 we depict the absorbance (a), reflectance (b), and transmittance (c), as function of frequency, for different values of r , from $r = 0.1$ up to $r = 0.6$, and keeping $d = h$, that is the limit of deep grooves. As r increases the position of the resonance shifts to the left. This happens because the width of the dielectric underneath graphene is increasing with r . Then, according to Eq. (46), the effective dielectric constant of the system increases, following from Eq. (45) that the resonance shifts toward lower energies. In the case of $r = 0.6$ two resonances are seen in the frequency window considered. They correspond to the excitation of surface plasmon-polaritons of wave numbers $2\pi/d$ and $4\pi/d$. Then, according to Eq. (45), the position of the second resonance should be $\sqrt{2}$ times

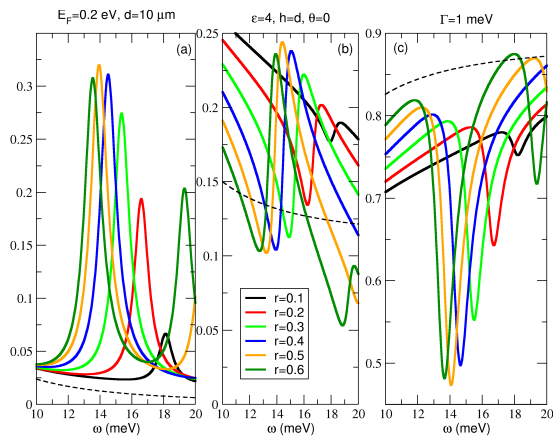


FIG. 4: Absorbance (a), reflectance (b), and transmittance (c) at normal incidence. The parameters are $E_F = 0.2$ eV, $d = 10$ μm , $h = d$, $\theta_i = 0$, $\epsilon_r = 4$, and $\Gamma = 1$ meV. The thin dashed line is the case $r = 1$.

the first resonance frequency. From the figure, the energy of the first resonance is $\hbar\omega = 13.6$ meV, while that of the second one is $\hbar\omega = 19.3$ meV; now we note that $\sqrt{2} \times 13.6 = 19.2$ meV, in agreement with the numerical result. We also note that the absorption of graphene is largest when $r = 0.5$, the symmetric case ($1 - d = 0.5$), reaching a value higher than 30%. Although we do not show it here, we have found that the absorption grows monotonically with increasing h and attains a maximum at a value larger than 45% for $h = 2d$.

Finally, we note that the reflectance curves have Fano-type shape.³⁹ This is due to the coupling of the external radiation field with the excitation of Bragg modes of surface plasmon-polaritons in periodically modulated structures.

An important quantity when dealing with plasmonic effects is the enhancement of the electromagnetic field close to the interface of the metal (in this case graphene) and the dielectric (the square-wave grating). The spatial intensity of the diffracted electromagnetic field from graphene is depicted in Fig.5. For the case off-resonance [Fig.5(a)] the magnetic field has a relatively small amplitude and is almost homogeneous along x -axis, while along z -axis exhibits a discontinuity at the plane $z = 0$ occupied by the graphene layer, in accordance with the boundary conditions.

The situation changes dramatically when the incident wave frequency coincides with that of a surface plasmon-polariton resonance [Figs.5(b-d)]. In this case the amplitude of the electromagnetic field in the vicinity of the graphene layer drastically increases. The electromagnetic field amplitude is maximal when the surface plasmon-polariton resonance occurs for the first harmonic [Fig.5(b)], that is for $q = 2\pi/d$, while it gradually decreases as the harmonic's order increases (compare with Fig.5(c) for second and Fig.5(d) for third harmon-

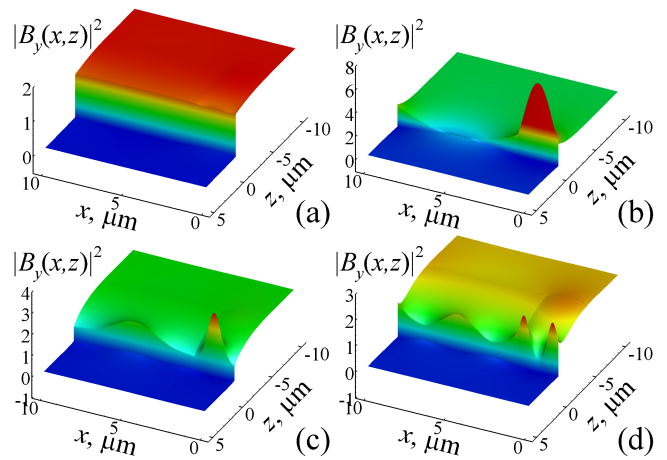


FIG. 5: Spatial dependence of the magnetic field $|B_y(x,z)|^2$, diffracted from the graphene layer on top of the square-wave grating. We have considered a groove depth $h = d/2$ and different frequencies of the incident wave: $\hbar\omega = 13$ meV (a), $\hbar\omega = 16$ meV (b), $\hbar\omega = 23$ meV (c) and $\hbar\omega = 28.4$ meV (d). The other parameters of the structure are the same as in Fig. 3

ics, respectively). It is this enhancement of the electromagnetic field due to the excitation of surface plasmon-polaritons in the vicinity of a metallic interface that is at the heart of sensing devices.

VI. MODULATED DOPING: A SIMPLE MODEL

As discussed in the Introduction, doping graphene using a bottom gate when the material lies on a grating leads to a position dependent conductivity, which is periodic along the x -direction. In this section we consider a simple model where, in addition to the grating itself, the conductivity is position dependent and periodic. In our model the conductivity is given by³⁸

$$\sigma(x) = \sigma_D \left(1 - \kappa \sin \frac{2\pi x}{d}\right), \quad (50)$$

where κ is a parameter controlling the degree of inhomogeneity. We also take $r = 0.5$ in our figures. This particular choice of r and $\sigma(x)$ makes the latter commensurate with the profile of the grating. From the point of view of the calculation we have to replace σ_D by $\sigma(x)$ in the formulas given above. The conductivity is then expanded in Fourier series as

$$\sigma(x) = \sum_{p=-\infty}^{\infty} \sigma_p e^{i2\pi p x/d}, \quad (51)$$

where

$$\sigma_p = \frac{1}{d} \int_0^d dx \sigma(x) e^{-i2\pi p x/d}. \quad (52)$$

For the case of the profile defined in Eq. (50) the Fourier series reduces to three terms only, those referring to

$p = 0, \pm 1$. A non-sinusoidal profile for $\sigma(x)$ will have more harmonics than just these three. Therefore, our model can also be considered the first term in the Fourier expansion of a more complex profile for $\sigma(x)$.

Relatively to the previous case of homogeneous conductivity, what changes in the equations is the form of the function $g_{\ell m}^{(\pm)}$, which now reads

$$g_{\ell m}^{(\pm)} = \left(\chi_{\ell m} \mp \frac{\sigma_D}{\omega} h_{\ell m} \Lambda_{\ell} \mp \epsilon_0 \Omega_{\ell m} \frac{\Lambda_{\ell}}{\beta_m^{(1)}} \right) e^{\pm i \Lambda_{\ell} h}, \quad (53)$$

where

$$h_{\ell m} = \Omega_{\ell m} - \frac{\kappa}{2i} \Omega_{\ell m+1} + \frac{\kappa}{2i} \Omega_{\ell m-1}. \quad (54)$$

The results for the absorbance, reflectance, and trans-

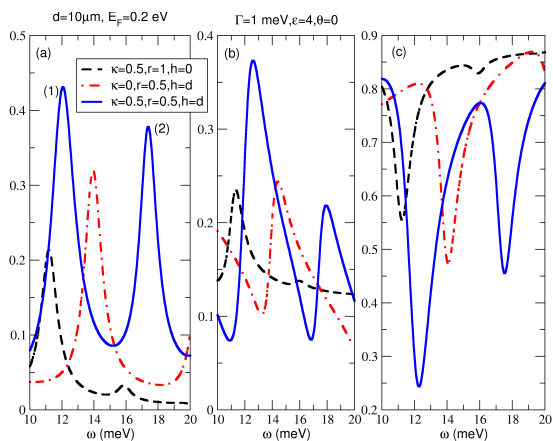


FIG. 6: Absorbance (a), reflectance (b), and transmittance (c) at normal incidence. Three distinct situations are considered: inhomogeneous conductivity, with grating (solid line) and without grating (dashed line), and homogeneous conductivity with grating (dotted-dashed line). Other parameters as in Fig. 4.

mittance are given in Fig. 6, considering the case where $\kappa = 0.5$, a fairly large value, corresponding to deep grooves. The dashed line is the case where graphene has an inhomogeneous conductivity on top of a homogeneous dielectric (i.e., no grating). (This situation is artificial and is only included for the sake of comparison.) Two resonant peaks can be seen, with the second peak being much smaller than the one at lower energies. The dashed-dotted line is the case where we have homogeneous graphene on the grating, and the solid line corresponds to the case where we have graphene with an inhomogeneous conductivity on the grating. The main effect is a shift of the position of the resonant peaks toward lower energies and an enhancement of the absorption, which bears its origin on the combined effect of the grating and of the periodic modulation of the conductivity. In the absorbance panel the energy of the resonance

labelled (2) is $\sqrt{2}$ larger than that of the resonance (1). Thus, the first resonance corresponds to an excitation of a surface plasmon-polariton of wave number $q = 2\pi/d$ whereas the second peak corresponds to the excitation of surface plasmon-polariton of wave number $q = 4\pi/d$. When we compare the dashed curve to the solid one we also note the prominence of the second plasmonic peak in the latter case, which is almost as intense as the low energy one. This is a consequence of the square profile and the dielectric nature of the grating. In metallic gratings the permittivity has a strong frequency dependence favouring the occurrence of the most intense plasmonic resonances at lower energies.⁴⁰

VII. CONCLUSIONS AND FUTURE WORK

We have shown that a flat sheet of graphene on top of a square-wave grating exhibits strong plasmonic behavior. With the help of the grating one can create a surface plasmon-polariton resonance. The effect is more pronounced in the case of deep grooves, where absorbances higher than 45% are attainable. We note that the parameter d is easy to control experimentally, providing a convenient way of tuning the position of the plasmonic resonance. The reflectance curves show a Fano-type line shape, which is manifest of the coupling of the external electromagnetic field (with a continuum of modes) to the surface plasmons in graphene (occupying a relatively narrow spectral band). The calculations we have performed assume that graphene is homogeneously doped (excluding Sec. VI), which is a crude approximation for the case of a bottom gate configuration of graphene doping. Therefore, our results are only directly applicable to the cases of either chemical doping or doping by a top gate. This type of gating is within the state-of-the-art.⁶⁴ In the particular case of bottom gate, we have to consider both the effect of inhomogeneous doping and the effect of strain (if the grooves are not filled with another dielectric). Both effects result in a position dependent conductivity. Then, the calculation of the properties of surface plasmon-polaritons requires the evaluation of the doping profile and the strain field. Once these are determined, one can use a Fourier expansion of the graphene conductivity as we have considered in our phenomenological model. As these preliminary results show, the coupling of the external wave to the surface plasmon-polaritons can be significantly enhanced in the presence of both the dielectric grating and periodic modulation of the conductivity. Detailed calculations for realistic graphene conductivity profiles are the goal of a future work.

Acknowledgements

NMRP acknowledges Bao Qiaoliang, José Viana-Gomes, and João Pedro Alpuim for fruitful discus-

sions. A. F. was supported by the National Research Foundation–Competitive Research Programme award “Novel 2D materials with tailored properties: beyond graphene” (Grant No. R-144-000-295-281). This work was partially supported by the Portuguese Foundation for Science and Technology (FCT) through Projects PEst-C/FIS/UI0607/2011 and PTDC-FIS-113199-2009.

Appendix A: Explicit form of $\chi_{\ell m}$

The calculation of the integral in Eq. (40) has to be divided into two pieces. The function $\chi_{\ell m}$ can be written as

$$\chi_{\ell m} = \chi_{\ell m}^{(1)} + \chi_{\ell m}^{(2)}, \quad (\text{A1})$$

where

$$\begin{aligned} \chi_{\ell m}^{(1)} = & -i \frac{A_2 a}{d(k_1 - \alpha_m)} (e^{i(k_1 - \alpha_m)d} - e^{i(k_1 - \alpha_m)rd}) \\ & + i \frac{A_2 c}{d(k_1 + \alpha_m)} (e^{-i(k_1 + \alpha_m)d} - e^{-i(k_1 + \alpha_m)rd}) \\ & - i \frac{B_2 b}{d(k_1 - \alpha_m)} (e^{i(k_1 - \alpha_m)d} - e^{i(k_1 - \alpha_m)rd}) \\ & + i \frac{B_2 f}{d(k_1 + \alpha_m)} (e^{-i(k_1 + \alpha_m)d} - e^{-i(k_1 + \alpha_m)rd}) \end{aligned} \quad (\text{A2})$$

and

$$\begin{aligned} \chi_{\ell m}^{(2)} = & -i \frac{A_2}{d(k_2 - \alpha_m)} (e^{i(k_2 - \alpha_m)dr} - 1) \\ & + i \frac{B_2}{d(k_2 + \alpha_m)} (e^{-i(k_2 + \alpha_m)dr} - 1). \end{aligned} \quad (\text{A3})$$

Since the square profile has a piecewise structure, the function $\Omega_{\ell m}$ is obtained directly from the function $\chi_{\ell m}$ as

$$\Omega_{\ell m} = \frac{\chi_{\ell m}^{(1)}}{\epsilon_0} + \frac{\chi_{\ell m}^{(2)}}{\epsilon_r \epsilon_0}. \quad (\text{A4})$$

Appendix B: Polaritonic spectrum

The polaritonic spectrum, $\hbar\omega(q)$, of the surface plasmons-polaritons (SPP) in graphene on a square-wave grating is represented in Fig.7, where $q = k_0 \sin \theta_i$ is the Bloch wavenumber. Here, and in order to avoid the appearance of an imaginary part of the eigenvalues, corresponding to surface plasmon-polariton damping, we considered graphene without disorder ($\Gamma = 0$). As expected, the periodicity of the grating induces a band structure in the SPP spectrum of graphene, showing energy gaps. At the same time, for normal incidence ($q = 0$) the frequency of the second band ($\hbar\omega \approx 15.85$ meV) almost coincides with the numerically obtained resonant frequency $\hbar\omega \approx 15.9$ meV. A similar good agreement happens for the frequency of fifth band and that of second resonance ($\hbar\omega \approx 23.1$ meV and $\hbar\omega \approx 23$ meV, respectively), as well as for frequency of sixth band and that of third resonance ($\hbar\omega \approx 28.3$ meV and $\hbar\omega \approx 28.4$ meV, respectively).

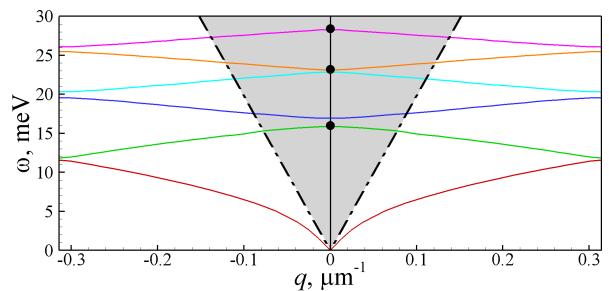


FIG. 7: Spectrum of surface plasmons-polaritons in graphene on a square-wave grating. We have considered $E_F = 0.2$ eV and $\Gamma = 0$. The other parameters are: $d = 10 \mu\text{m}$, $r = 0.25$, $\epsilon_r = 4$. The gray region represents the “light cone”, limited by the light lines $\omega = c|q|$ (dash-dotted lines), inside which the excitation of surface plasmons-polaritons by incident light is possible. The frequencies, corresponding to the numerically obtained resonant minima of the transmittance for normal incidence, $\theta_i = 0$, are represented by black circles on the line $q = 0$.

¹ A. H. Castro Neto, F. Guinea, N. M. R. Peres, K. S. Novoselov, and A. K. Geim, *Rev. Mod. Phys.* **81**, 109 (2009).
² N. M. R. Peres, *Rev. Mod. Phys.* **82**, 2673 (2010).
³ S. D. Sarma, S. Adam, E. H. Hwang, and E. Rossi, *Rev. Mod. Phys.* **83**, 407 (2011).
⁴ N. M. R. Peres, F. Guinea, and A. H. Castro Neto, *Phys. Rev. B* **73**, 125411 (2006).
⁵ L. A. Falkovsky and S. S. Pershoguba, *Phys. Rev. B* **76**, 153410 (2007).
⁶ T. Stauber, N. M. R. Peres, and F. Guinea, *Phys. Rev. B* **76**, 205423 (2007).
⁷ T. Stauber, N. M. R. Peres, and A. H. Castro Neto, *Phys. Rev. B* **78**, 085418 (2008).
⁸ T. Stauber, N. M. R. Peres, and A. K. Geim, *Phys. Rev.*

B **78**, 085432 (2008).
⁹ V. P. Gusynin, S. G. Sharapov, and J. P. Carbotte, *New J. Phys.* **11**, 095013 (2009).
¹⁰ A. G. Grushin, B. Valenzuela, and M. A. H. Vozmediano, *Phys. Rev. B* **80**, 155417 (2009).
¹¹ E. G. Mishchenko, *Phys. Rev. Lett.* **103**, 246802 (2009).
¹² L. Yang, J. Deslippe, C.-H. Park, M. L. Cohen, and S. G. Louie, *Phys. Rev. Lett.* **103**, 186802 (2009).
¹³ N. M. R. Peres, R. M. Ribeiro, and A. H. Castro Neto, *Phys. Rev. Lett.* **105**, 055501 (2010).
¹⁴ A. Ferreira, J. Viana-Gomes, Y. V. Bludov, V. M. Pereira, N. M. R. Peres, and A. H. Castro Neto, *Phys. Rev. B* **84**, 235410 (2011).
¹⁵ J.-T. Liu, N.-H. Liu, J. Li, X. J. Li, and J.-H. Huang, *Appl. Phys. Lett.* **101**, 052104 (2012).

- ¹⁶ M. Busl, G. Platero, and A.-P. Jauho, *Phys. Rev. B* **85**, 155449 (2012).
- ¹⁷ R. R. Nair, P. Blake, A. N. Grigorenko, K. S. Novoselov, T. J. Booth, T. Stauber, N. M. R. Peres, and A. Geim, *Science* **320**, 1308 (2008).
- ¹⁸ A. B. Kuzmenko, E. van Heumen, F. Carbone, and D. van der Marel, *Phys. Rev. Lett.* **100**, 117401 (2008).
- ¹⁹ K. F. Mak, M. Y. Sfeir, Y. Wu, C. H. Lui, J. A. Misewich, and T. F. Heinz, *Phys. Rev. Lett.* **101**, 196405 (2008).
- ²⁰ Z. Q. Li, E. Henriksen, Z. Jiang, Z. Hao, M. C. Martin, P. Kim, H. Stormer, and D. Basov, *Nature Phys.* **4**, 532 (2008).
- ²¹ F. Wang, Y. Zhang, C. Tian, C. Girit, A. Zettl, M. Crommie, and Y. R. Shen, *Science* **320**, 206 (2008).
- ²² A. B. Kuzmenko, I. Crassee, D. van der Marel, P. Blake, and K. S. Novoselov, *Phys. Rev. B* **80**, 165406 (2009).
- ²³ I. Crassee, J. Levallois, A. L. Walter, M. Ostler, A. Bostwick, E. Rotenberg, T. Seyller, D. van der Marel, and A. B. Kuzmenko, *Nat. Phys.* **7**, 48 (2011).
- ²⁴ Q. Bao, H. Zhang, B. Wang, Z. Ni, C. H. Y. X. Lim, Y. Wang, D. Y. Tang, and K. P. Loh, *Nature Photonics* **5**, 411 (2011).
- ²⁵ J. M. Dawlaty, S. Shivaraman, J. Strait, P. George, M. Chandrashekar, F. Rana, M. G. Spencer, D. Veksler, and Y. Chen, *Appl. Phys. Lett.* **93**, 131905 (2008).
- ²⁶ H. Yan, F. Xia, W. Zhu, M. Freitag, C. Dimitrakopoulos, A. A. Bol, G. Tulevski, and P. Avouris, *ACS Nano* **5**, 9854 (2011).
- ²⁷ L. Ren, Q. Zhang, S. Nanot, I. Kawayama, M. Tonouchi, and J. Kono, *Journal of Infrared, Millimeter, and Terahertz Waves* **33**, 846 (2012).
- ²⁸ L. Ren, Q. Zhang, J. Yao, Z. Sun, R. Kaneko, Z. Yan, S. L. Nanot, Z. Jin, I. Kawayama, M. Tonouchi, et al., *Nano Lett.* **12**, 3711 (2012).
- ²⁹ M. Tonouchi, *Nature Photonics* **1**, 97 (2007).
- ³⁰ H. Yan, X. Li, B. Chandra, G. Tulevski, Y. Wu, M. Freitag, W. Zhu, P. Avouris, and F. Xia, *Nature Nano.* **7**, 330 (2012).
- ³¹ J. Chen, M. Badioli, P. Alonso-Gonzalez, S. Thongrattanasiri, F. Huth, J. Osmond, M. Spasenovic, A. Centeno, A. Pesquera, P. Godignon, et al., *Nature* **487**, 77 (2012).
- ³² G. Konstantatos, M. Badioli, L. Gaudreau, J. Osmond, M. Bernechea, P. G. de Arquer, F. Gatti, and F. H. L. Koppens, *Nature Nanotechnology* **7**, 363 (2012).
- ³³ Z. Fei, G. O. Andreev, W. Bao, L. M. Zhang, A. S. McLeod, C. Wang, M. K. Stewart, Z. Zhao, G. Dominguez, M. Thiemens, et al., *Nano Lett.* **11**, 4701 (2011).
- ³⁴ Z. Fei, A. S. Rodin, G. O. Andreev, W. Bao, A. S. McLeod, M. Wagner, L. M. Zhang, Z. Zhao, G. Dominguez, M. Thiemens, et al., *Nature* **487**, 82 (2012).
- ³⁵ L. Vicarelli, M. S. Vitiello, D. Coquillat, A. Lombardo, A. C. Ferrari, W. Knap, M. Polini, V. Pellegrini, and A. Tredicucci, *Nature Materials* **11**, 865 (2012).
- ³⁶ I. Crassee, M. Orlita, M. Potemski, A. L. Walter, M. Ostler, T. Seyller, I. Gaponenko, J. Chen, and A. B. Kuzmenko, *Nano Lett.* **12**, 2470 (2012).
- ³⁷ T. J. Echtermeyer, L. Britnell, P. K. Jasnós, A. Lombardo, R. V. Gorbachev, A. N. Grigorenko, A. K. Geim, A. C. Ferrari, and K. S. Novoselov, *Nature Communications* **2**, 458 (2011).
- ³⁸ N. M. R. Peres, A. Ferreira, Y. V. Bludov, and M. I. Vasilevskiy, *J. Phys.: Condens. Matter* **24**, 245303 (2012).
- ³⁹ Y. V. Bludov, N. M. R. Peres, and M. I. Vasilevskiy, *Phys. Rev. B* **85**, 245409 (2012).
- ⁴⁰ A. Ferreira and N. M. R. Peres, *Phys. Rev. B* **86**, 205401 (2012).
- ⁴¹ W. Gao, J. Shu, C. Qiu, and Q. Xu, *ACS Nano* **6**, 7806 (2012).
- ⁴² A. Ferreira, N. M. R. Peres, R. M. Ribeiro, and T. Stauber, *Phys. Rev. B* **85**, 115438 (2012).
- ⁴³ M. Furchi, A. Urich, A. Pospischil, G. Lilley, K. Unterrainer, H. Detz, P. Klang, A. M. Andrews, W. Schrenk, G. Strasser, et al., *Nano Letters* **12**, 2773 (2012).
- ⁴⁴ A. A. Dubinov, V. Y. Aleshkin, V. Mitin, T. Otsuji, and V. Ryzhii, *J. Phys.: Condens. Matter* **23**, 145302 (2011).
- ⁴⁵ J. Zhang, L. Zhang, and W. Xu, *J. Phys. D: Appl. Phys.* **45**, 113001 (2012).
- ⁴⁶ A. N. Grigorenko, M. Polini, and K. S. Novoselov, *Nature Photonics* **6**, 749 (2012).
- ⁴⁷ P. Tassin, T. Koschny, M. Kafesaki, and C. M. Soukoulis, *Nature Photonics* **6**, 259 (2012).
- ⁴⁸ F. Bonaccorso, Z. Sun, T. Hasan, and A. C. Ferrari, *Nature Photonics* **4**, 611 (2010).
- ⁴⁹ Q. Bao and K. P. Loh, *ACS Nano* **6**, 3677 (2012).
- ⁵⁰ B. Sensale-Rodriguez, R. Yan, S. Rafique, M. Zhu, W. Li, X. Liang, D. Gundlach, V. Protasenko, M. M. Kelly, D. Jena, et al., *Nano Lett.* **12**, 4518 (2012).
- ⁵¹ Y. V. Bludov, M. I. Vasilevskiy, and N. M. R. Peres, *EuroPhys. Lett.* **92**, 68001 (2010).
- ⁵² Y. V. Bludov, M. I. Vasilevskiy, and N. M. R. Peres, *J. Appl. Phys.* **112**, 084320 (2012).
- ⁵³ Y. Zhou and M. W. Wu, *Phys. Rev. B* **83**, 245436 (2011).
- ⁵⁴ S. A. Mikhailov, *Europhys. Lett.* **79**, 27002 (2007).
- ⁵⁵ S. A. Mikhailov and K. Ziegler, *J. Phys.: Condens. Matter* **20**, 384204 (2008).
- ⁵⁶ S. A. Mikhailov, *Microelectronics Journal* **40**, 712 (2009).
- ⁵⁷ L. A. Falkovsky, *J. Phys.: Conf. Ser.* **129**, 012004 (2008).
- ⁵⁸ J. Horng, C.-F. Chen, B. Geng, C. Girit, Y. Zhang, Z. Hao, H. A. Bechtel, M. Martin, A. Zettl, M. F. Crommie, et al., *Phys. Rev. B* **83**, 165113 (2011).
- ⁵⁹ J. Chandezon, D. Maystre, and G. Raoult, *J. Optics* **11**, 235 (1980).
- ⁶⁰ L. Li, J. Chandezon, G. Granet, and J.-P. Plumey, *Applied Optics* **38**, 304 (1999).
- ⁶¹ P. Sheng, R. S. Stepleman, and P. N. Sanda, *Phys. Rev. B* **26**, 2907 (1982).
- ⁶² S. Tongay, K. Berke, M. Lemaitre, Z. Nasrollahi, D. B. Tanner, A. F. Hebard, and B. R. Appleton, *Nanotechnology* **22**, 425701 (2011).
- ⁶³ H. Liu, Y. Liu, and D. Zhu, *J. Mater. Chem.* **21**, 3335 (2011).
- ⁶⁴ L. Ju, B. Geng, J. Horng, C. Girit, M. C. Martin, Z. Hao, H. A. Bechtel, X. Liang, A. Zettl, Y. R. Shen, et al., *Nature Nanotechnology* **6**, 630 (2011).